

Novel Approaches for Minutiae Filtering in Fingerprint Images

Abstract

Minutiae extraction is one of the critical steps in fingerprint verification algorithms. Any missing minutiae or spurious minutiae introduced at this stage can degrade the performance of the matching algorithm. Existing structural approaches for minutiae filtering use heuristics and adhoc rules to eliminate such false positives, where as gray level approaches are based on using raw pixel values and a supervised classifier such as neural networks. We propose two new techniques for minutiae verification based on non-trivial gray level features. The proposed features intuitively represents the structural properties of the minutiae neighborhood leading to better classification. We use directionally selective steerable wedge filters to differentiate between minutiae and non-minutiae neighborhoods with reasonable accuracy. We also propose a second technique based on Gabor expansion that results in even better discrimination. We present an objective evaluation of both the algorithms. Apart from minutiae verification, the feature description can also be used for minutiae detection and minutiae quality assessment.

1 Introduction

Fingerprint verification has emerged as one of the most reliable means of biometric authentication due to its universality, distinctiveness, permanence and accuracy [15]. Contrary to popular belief, inspite of its long history and extensive research efforts, automated fingerprint recognition is not a closed problem. Reliable matching of fingerprints is a challenging problem. No two different impressions of the fingerprint are identical even when they come from the same individual. The matching algorithm has to be therefore invariant to changes in orientation, displacement, elastic deformation, occlusion and missing features. Varying skin conditions may lead to poor quality images that can lead to feature extraction errors and subsequently error during recognition.

Most of the existing fingerprint recognition algorithms can be categorized into the following approaches [15]. (i) Correlation based matching : In this approach the similarity between two fingerprints is obtained using correlation. The correlation may be performed in the spatial or Fourier domain or using high-speed optical correlators [4, 22, 20]. Invariance to rotation and displacement is achieved by aligning the fingerprint images at multiple orientations and dis-

placements. However, this technique cannot handle variations in brightness and ridge quality. (ii) Ridge feature based matching : These algorithms depend on extracting texture, shape, frequency orientation and other ridge characteristics for matching. Previous work by Jain et. al [11, 12] provide more details on this approach. (iii) Minutiae based matching: These techniques are by far the most widely used in existing fingerprint matching algorithms. Given a fingerprint image, all the minutiae locations, orientations and structural relationship among the points are determined and stored as part of the template. During matching, the deformation between two such point sets is recovered and the point correspondences are determined to generate a similarity score [15].

Many of the minutiae extraction algorithms are sequential resulting in error propagation in each of the stages. Error resulting from poor quality images can be eliminated using enhancement techniques [10]. Other variations due to displacement and elastic deformation are handled by the matching algorithm. In this paper, we try to by eliminate errors introduced during the feature extraction stage. Figure 1 illustrates instances of false positivies detected by a typical feature extraction algorithm. The feature extraction stages results in the following type of errors (i) Missing minutiae: The feature extraction algorithm fails to detect existing minutia when the minutiae is obscured by surrounding noise or poor ridge structures. (ii) Spurious minutia: The feature extraction algorithm falsely identifies a noisy ridge structure such as a crease, ridge break or gaps as minutiae. The types of errors introduced in this case strongly depend on the feature extraction process. When the feature extraction is performed using binarization and thinning, spurs, bridges, opposing minutiae, triangles, ladders are some of the structures leading to false minutiae detection [15]. Gray level based feature extraction methods such as the ridge following approach proposed by Maio and Maltoni [14] can eliminate many of the sources of error that are caused by binarization and thinning. However, in poor contrast or poor quality images where the local maxima cannot be reliably located, false positives are still introduced. Therefore a post-processing step is required where such spurious minutiae features are eliminated. It has been shown that feature refinement can result in considerable improvement in the accuracy of a minutia based matching algorithm [16].

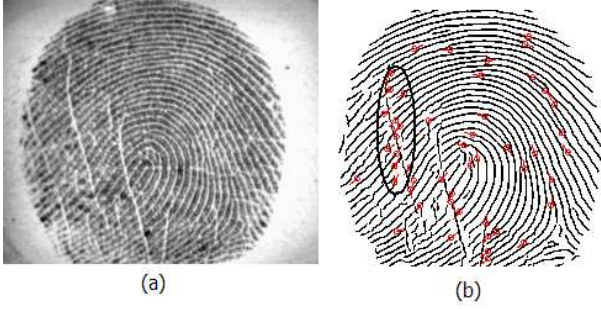


Figure 1: Fingerprint image with minutiae extracted using our algorithm. Some of the spurious minutiae occurring along the creases has been highlighted

1.1 Prior related work

Errors introduced due to missing minutiae cannot be corrected using post processing steps. However, many of the false positivies introduced during feature extraction can be removed using pruning methods. Existing methods to filter spurious minutiae can be categorized into two methods(i) Structural post processing and (ii) Gray level image based filtering. Structural post processing methods prune spurious minutia based on heuristics rules that use the relative location of the detected minutia, length of the ridges, relative orientation of the minutiae among other structural information. However, these rules are very specific to the feature extraction algorithm. Xiao and Raafat [23] provided taxonomy of structures resulting from thinning that lead to spurious minutia and proposed heuristic rules to eliminate them. Hung [5] proposed a graph-based algorithm that exploits the duality of the ridges and bifurcation. The binarization and thinning is carried on positive and negative gray level images resulting in ridge skeleton and its complementary valley skeleton. Minutiae features that occur in both images are retained while eliminating the false positivies. Gray scale based techniques use the gray scale values in the immediate neighborhood to verify the presence of a real minutia. Prabhakar et. al [16] proposed a gray scale image based approach to eliminate false minutiae. A 64x64 region of the neighborhood surrounding the minutiae is normalized w.r.t orientation and brightness variation. Horizontatally oriented Gabor filters are used to enhance the region and the pixels in the central 32x32 regions is used as features to distinguish between minutiae and non-minutiae neighborhoods. The classification is done using a Learning Vector Quantizer that uses the central 1024 pixels as input and classifies the region as ridge, bifurcation or non-minutiae. Maio and Maltoni [6] proposed a neural network based approach for minutiae filtering. In this method, the minutiae neighhborhood is normalized w.r.t ridge frequency in addition to orientation and brightness variations. The dimensionality of the feature set is reduced by

projecting the gray scale image on to a set of basis images derived using Karhunen Leove Transform. Classification is done using a shared weights neural network that uses both positive and negative images of the minutiae neighborhood to exploit the duality of the ridge and bifurcation. Although this approach leads to significant reduction in the number of false positivies and exchanged minutiae, it also increases the number of missing minutiae. Both the mentioned approaches improve the matching performance when the minutia filtering is used as a post-processing after feature extraction. But it is does not indicate the exact underlying mechanism or the features that discriminate between minutiae and non minutiae neighborhoods. However, it can be seen that the use of neural networks in both these approaches indicates to the use of template matching as the underlying mechanism.

1.2 Overview

Minutiae represent local deviation in the flow of ridges. Although many different types of fingerprint features have been identified, ridge endings and bifurcation account for a majority of those features. We treat both ridge endings and bifurcation uniformly since their type can get exchanged with slight variation of pressure. Also, the majority of the existing fingerprint matching algorithms do not distinguish between the minutia types during verification. We propose two feature descriptors that can be used to differentiate between minutiae and non minutiae neighborhoods. The first approach is based on the response of the minutiae neighborhood to a bank of steerable wedge filters. The response is fed to a feedforward back propagation network to classify the inputs as either minutiae or non minutiae neighborhood. The second and also the more accurate approach is based expressing the minutiae neighborhoods as a linear sum of basis images made up of multi-resolution Gabor elementary functions. The rest of the paper is organized as follows. Section 2 explains the use of wedge filter for minutiae verification. The second approach using Gabor expansion is presented in section 3. Experimental verification and objective evaluation of the techniques is presented in section 4. Finally conclusion and future work are discussed in section 5.

2 Steerable Wedge Filters

Steerable filters have been used for some time to analyze local orientation in images. Steerable filters allow us to compute the responses at different orientation as a linear combination of response to a set of basis filters. Freeman and Aldeson [9] first developed the concept of steerable filters. They used directional derivatives of Gaussians to construct these filters. However, the symmetry of these derivatives imposes an angular periodicity π of on these filter responses irrespective of the basic image structure. The bimodal response is not very

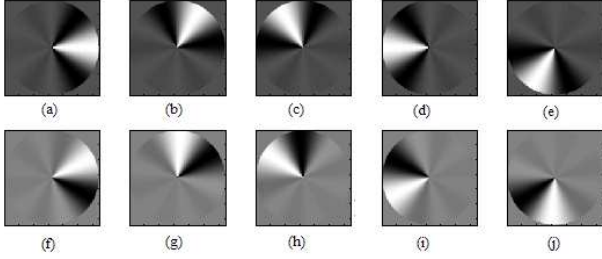


Figure 2: Steerable wedge filters for $N=5$ (a)-(e) evenly symmetric filters, (f)-(j) oddly symmetric filters

useful in junction analysis and pattern recognition application where a full range resolution ($[0, 2\pi]$) is needed. Simoncelli and Farid [21] propose asymmetrical filters that exhibit a unimodal response. A brief overview of these filters is provided for completeness. Further details are provided in [9] and [21]. Consider a bank of two filters given by

$$G_n^0(r, \theta) = \cos(\theta) \frac{\partial g^n(r)}{\partial r^n} \quad (1)$$

$$G_n^{\pi/2}(r, \theta) = \sin(\theta) \frac{\partial g^n(r)}{\partial r^n} \quad (2)$$

$$g(r) = e^{-\frac{r^2}{2}} \quad (3)$$

The subscript indicates the order of the derivative while the superscript indicates the orientation of the basis filters. It can be easily shown that using these two basis filters, a filter oriented in an arbitrary direction ϕ can be constructed using

$$G_n^\phi = G_n^0 \cos(\phi) + G_n^{\pi/2} \sin(\phi) \quad (4)$$

$\cos(\phi)$ and $\sin(\phi)$ form the interpolation function. Generalizing, it can be shown [9] that in order to express the angular response at any orientation ϕ using $2\hat{N}$ filters, it is sufficient that the angular filter contains a weighted sum of the first \hat{N} harmonics. Simoncelli et. al [21] further impose a hilbert transform relation between the even and odd components of the filter. The filters are obtained using

$$h_e(\phi) = \sum_{n=1}^{\hat{N}} \omega_n \cos(n\phi) \quad (5)$$

$$h_o(\phi) = \sum_{n=1}^{\hat{N}} \omega_n \sin(n\phi) \quad (6)$$

The weights ω_n are chosen so as to localize the energy response. To construct a filter in arbitrary orientation, it is expressed as a linear combination of basis filters $h(\phi - \alpha_n)$. Both the even and odd filter can be expressed using the generalized steerability relation

$$f^\alpha(r, \phi) = h(\phi - \alpha)g(r) = g(r) \sum_{n=1}^{\hat{N}} k_n(\alpha)h(\phi - \alpha_n) \quad (7)$$

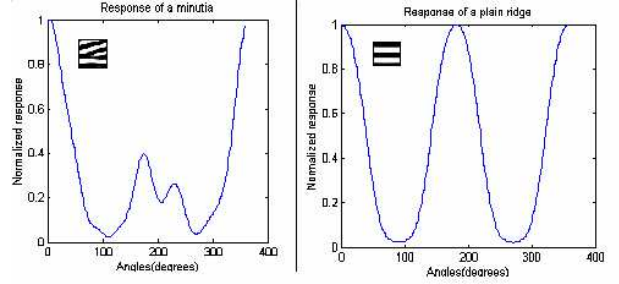


Figure 3: Response of the wedge filter to a prototypical bifurcation and plain ridge

$g(r)$ represents an arbitrary radial function with compact support. $k_n \alpha$ represents the interpolation function and α_n represents the orientations of the basis filters. 2 shows the basis filters for $N=5$. The angular response of the filter at different orientations is computed using the squared energy response of the even and odd symmetric filters and is given by

$$E(\phi) = h_e^2 + h_o^2$$

2.1 Minutiae Verification

Minutiae is marked by local deviation in the ridge flow, with three dominant local directions corresponding to the two branches of the bifurcation and the parallel ridge direction. Plain ridges are marked by a single dominant direction aligned with the horizontal. On the other hand, false positives encountered around the creases and noisy regions of the fingerprint are marked by multiple dominant directions. Creases, in particular are identified by dominant components in directions orthogonal to the ridge flow. However, such a distinction can be made in a very small neighborhood surrounding the minutiae. We observe that neighborhoods greater than 16×16 and 24×24 pixels cannot fully resolve these distinctions. Figure 3 shows response of a wedge filter to a prototypical bifurcation and non minutiae region. The distinction between the two regions is clearly evident. The advantage of this approach over using a set of oriented Gabor filter responses are as follows (i) Since the Gabor kernel is symmetric, it has a bimodal response with a period of π radians, where as the asymmetric wedge filter has a unimodal response spanning $[-\pi, \pi]$ radians. (ii) Steerable filters allows us to compute the response at any arbitrary orientation as a linear sum of responses to a set of fixed basis filters. With Gabor filters, this is possible only if we perform interpolation between a set of closely spaced filters. This would mean having a large set of oriented filters to begin with. (iii) The proposed approach is more computationally efficient, since the response at each orientation is obtained by projecting the image onto the basis function. This only involves computing the dot products as opposed to convolving the image using a

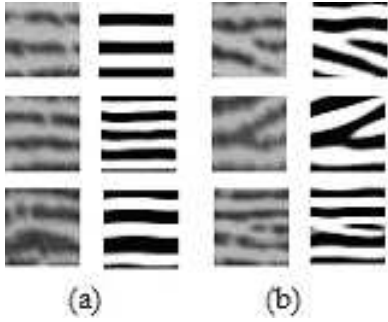


Figure 4: Response of the wedge filter to a prototypical bifurcation and plain ridge

set of Gabor kernels.

Minutiae verification using wedge filter consists of the following steps (i) A 24x24 region surrounding each potential minutiae is normalized w.r.t orientation. (ii) The local block is enhanced using the algorithm described in [1]. Figure 4 shows the results of the normalization. This makes it invariant to brightness and contrast variation. (iii) The orientation response of the block is computed in the interval $[-\pi, \pi]$ using $N=18$ basis filters. (iv) The responses are then classified into minutiae and non-minutiae region using a neural network classifier.

2.2 Neural Networks

An analysis using Fisher discriminant analysis [8] shows us that the two classes are not linearly separated. Therefore it requires a more sophisticated classification step. It is well known that a multi-layered feed forward neural network is capable of classifying non-linearly separated data. We use a three layered, 180-10-1 neuron architecture for our purpose. We use resilient back propagation [19] algorithm to train the network. It was found during our experiments that the resilient propagation network converges roughly more than 10 times faster than the simple back propagation algorithm and also compared to networks that include momentum parameter and adaptive learning rates. The resilient back propagation algorithm works by considering only the sign of the derivative for updating the weights. The change in weight is determined by a separate parameter. Therefore unlike gradient descent methods, the rate of convergence does not slow down as the slope of the error gradient decreases with time.

3 Gabor expansion

Gabor elementary functions have been previously used for enhancement of fingerprint images [10] and also for synthetic fingerprint generation [18]. They are also very important in the field neurobiology. It has been found that the

receptive field of the neurons in mammalian visual cortex can be accurately modeled using Gabor elementary functions [13]. Furthermore, they have important signal properties such as optimal joint space frequency resolution [17]. Daugman [7] and Lee [13] have used Gabor elementary functions as basis functions to represent generic 2D images. Gabor elementary functions form a very intuitive representation of fingerprint images since they capture the periodic, yet non-stationary nature of the fingerprint regions. However, unlike Fourier bases or discrete cosine bases, using Gabor elementary functions have the following problems. (i) From a signal processing point of view, they do not form a tight frame. This means that the image cannot be represented as a linear superposition of the Gabor elementary functions with coefficients derived by projecting the image onto the same set of basis functions. However, Lee [13] has derived conditions under which a set of self similar Gabor basis functions form a complete and approximately orthonormal set of basis functions. (ii) They are biorthogonal bases. This means that the basis functions used to derive the coefficients (analysis functions) and the basis functions used to reconstruct the image (synthesis functions) are not identical or orthogonal to each other. Bastiaans [3] has analytically derived the analysis functions for 1D when the synthesis functions are made up of modulated gaussian windows. However, Daugman proposes a simple optimization approach to obtain the coefficients.

Daugman gives the following form for the 2D Gabor elementary function

$$G(x, y) = \exp(-\pi[(x - x_0)^2\alpha^2 + (y - y_0)^2\beta^2]) \cdot \exp(-2\pi i[u_0(x - x_0) + v_0(y - y_0)]) \quad (8)$$

x_0 and y_0 represent the center of the elementary function in the spatial domain. u_0 and v_0 represent the modulation frequencies. α^2 and β^2 represent the variance along the major and minor axes respectively and therefore the extent of support in the spatial domain.

3.1 Feature representation

We use a multi-resolution representation using Gabor expansion to distinguish between minutiae and non minutiae neighborhood. The bases are derived using a self similar Gabor elementary functions computed at multiple scales and orientations. Figure 5 displays some of the basis functions used to derive the feature representation. The basis function at scale m , displacement $(p, q) \in (0, 2^m, 2^{2m}, \dots, N)$ and orientation θ is given by [7]

$$\Psi_{mpq\theta}(x, y) = 2^{-m}G(x', y') \quad (9)$$

$$x' = 2^{-m}[x \cos(\theta) + y \sin(\theta)] - p \quad (10)$$

$$y' = 2^{-m}[-x \sin(\theta) + y \cos(\theta)] - q \quad (11)$$

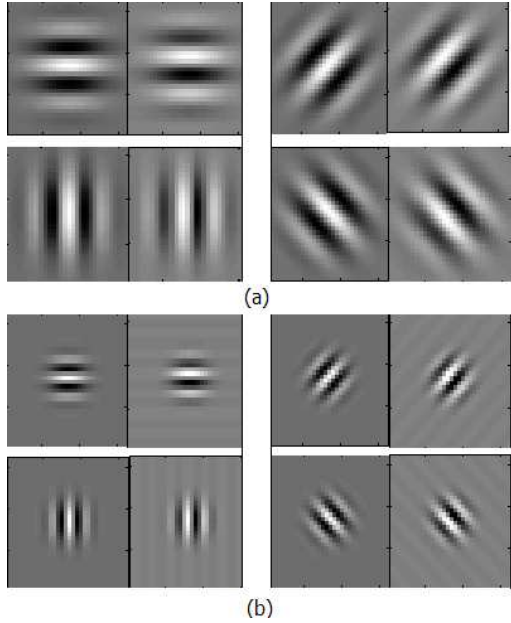


Figure 5: Some of the Gabor basis functions used to represent the minutiae neighborhoods

We represent a 32×32 region around the fingerprint image using basis functions that span two scales and four orientations resulting in 272 such basis functions. The image can therefore approximately be represented using

$$I(x, y) = \sum_{n=1}^{272} a_n G_n(x, y) \quad (12)$$

The optimal coefficients are obtained using a gradient descent approach as suggested by Daugman in [7]. At each iteration the coefficient is incremented by an amount

$$\Delta a_n = G_n(x, y) \cdot I(x, y) - G_n(x, y) \cdot \left(\sum_k G_k(x, y) I(x, y) \right) \quad (13)$$

Figure 6 shows examples of normalized minutiae neighborhoods and their approximate reconstruction using Gabor expansion.

3.2 Bayesian Classification

We use a deterministic Bayesian classifier [8] in order to distinguish between minutiae and non-minutiae neighborhoods. We can treat minutiae and non-minutiae as two states of nature ω_1 and ω_2 . The coefficients can be represented using a feature vector \vec{x} . We decide the given sample as belonging to ω_1 if the posterior probability $p(\omega_1|\vec{x})$ is greater than $p(\omega_2|\vec{x})$. According to Baye's rule, the posterior probabilities

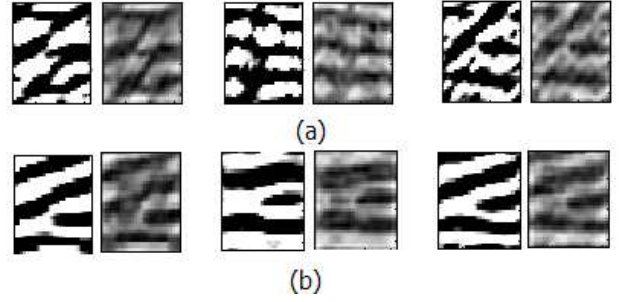


Figure 6: Some of the Gabor basis functions used to represent the minutiae neighborhoods

can be calculated using

$$p(\omega_i|\vec{x}) = \frac{p(\vec{x}|\omega_i)p(\omega_i)}{\sum_i p(\vec{x}|\omega_i)} \quad (14)$$

In practice, we usually take a decision that maximizes the log probabilities $\ln(p(\omega_i|\vec{x}))$. In terms of discriminant functions, we decide that the feature belongs to ω_1 if

$$g_1(\vec{x}) > g_2(\vec{x}) \quad (15)$$

where

$$g_i(\vec{x}) = \ln p(\vec{x}|\omega_i) + \ln p(\omega_i) \quad (16)$$

Also, we have observed that all conditional probabilities, $p(\vec{x}|\omega_i)$ can be represented as univariate gaussian. We further assume that the features are independent of each other. This conclusion was drawn after examining the covariance matrix of the feature distribution. Only 3% of feature combinations had correlation coefficient greater than 0.25. Furthermore, we also assume the prior probabilities $p(\omega_1)$ and $p(\omega_2)$ to be equal. The discriminant function can therefore be expressed as

$$g_i(\vec{x}) = -\frac{1}{2}(\vec{x} - \vec{\mu}_i)^t \Sigma_i^{-1} (\vec{x} - \vec{\mu}_i) - \frac{1}{2} \ln |\Sigma_i| \quad (17)$$

Here $\vec{\mu}_i$ represents the mean vector for the class ω_i and Σ_i consists of a diagonal covariance matrix since we assume each feature to be independent of each other.

3.3 Feature Selection

We notice that all the 272 features do not sufficiently discriminate the two classes ω_1 and ω_2 . We therefore consider only those features that *sufficiently discriminate among the classes*. We define the discriminability metric D of each feature x_i as

$$D_i = \frac{|\mu_{1i} - \mu_{2i}|}{\sigma_{1i} + \sigma_{2i}} \quad (18)$$

We select only those features where $D_i > 0.5$. This results in retaining 12 of the 272 total features. Only these features

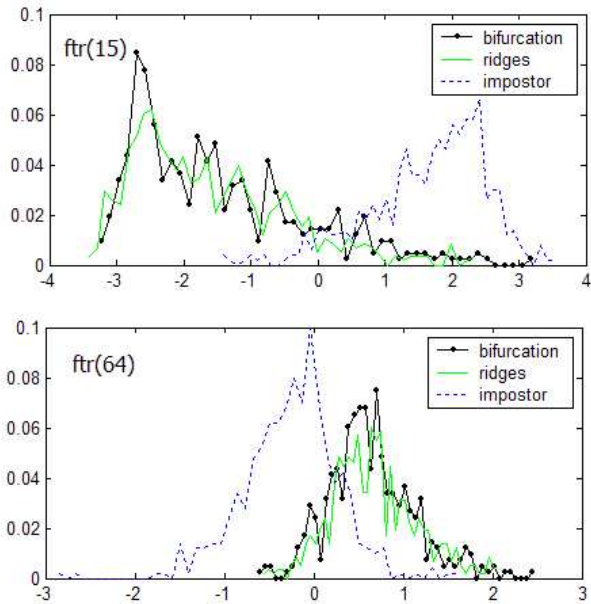


Figure 7: Distribution of the two most distinctive features

are used for the Bayesian classification. Figure 7 shows distribution of some of the features and the corresponding discriminability metric D .

4 Experimental Verification

4.1 Wedge filter approach

4.1.1 Test data

The test data consisted of 2000 genuine and impostor minutiae neighborhoods extracted out of 30 pairs of images. The ground truth minutiae location in these images were established manually using a semi-automated truthing tool. Half of these pairs consisted of *bad prints that contained poor ridge structure and creases*. The quality of the fingerprint images was established using an objective quality metric described in [2].

4.1.2 Training and Testing

The training set consists of 500 impostor and genuine neighborhoods that have been normalized w.r.t orientation and brightness. The testing set consists of an equal number of impostor and genuine neighborhoods. Ridges and bifurcation are treated uniformly since it can be empirically shown the response of the wedge filter are identical in each case. The 180 dimensional features obtained are used to train a neural network to distinguish between the two classes. The equal error rates during training and testing are 6% and 17% re-

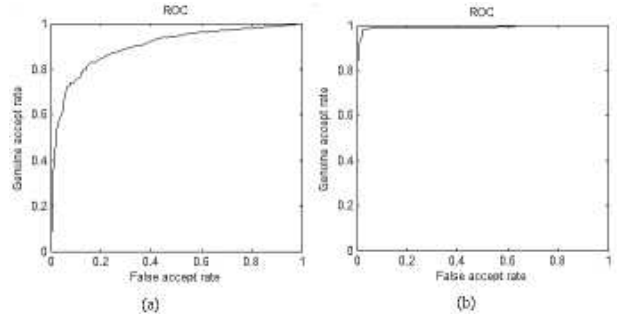


Figure 8: ROC for the (a) wedge feature classifier and (b) Gabor based classifier

spectively. Figure 8a shows the ROC curve for the wedge feature classifier.

4.2 Gabor expansion approach

4.2.1 Test data

The test data for the Gabor expansion based classifier consists of 1500 of the 2000 minutiae neighborhoods discussed previously. This consists of 415 are bifurcations, 585 are ridge endings and 500 are non-minutiae neighborhoods. The other 500 impostor neighborhoods were not used to have an unbiased dataset. The neighborhoods were normalized before feature extraction. Bifurcations are treated as negatives of the ridge endings and therefore the negative image is used during feature extraction. The 272 features are pruned using the procedure mentioned in section 3.3. The features are classified using Bayesian classification.

4.2.2 Training and testing

Training uses 60% of the data and the rest is used for testing. The training results in the following pieces of information. (i) The mean vectors $\vec{\mu}_i$ and $\vec{\mu}_r$, the std. deviation vectors $\vec{\sigma}_i$ and $\vec{\sigma}_r$ corresponding to impostor and genuine neighborhoods respectively. The equal error rate during training and testing are 2% and 2% respectively. Figure 8b shows the ROC curve for the Gabor expansion based classifier.

5 Conclusion

We have presented two novel features for minutiae verification in fingerprint images. The algorithm provides accuracy better than other gray scale approaches mentioned in literature. The approaches are computationally efficient and can also be used to design minutiae detector that can directly operate on the gray scale images. Our future work will involve fusing the decision of the two classifiers and studying the effects of minutiae verification on matching performance.

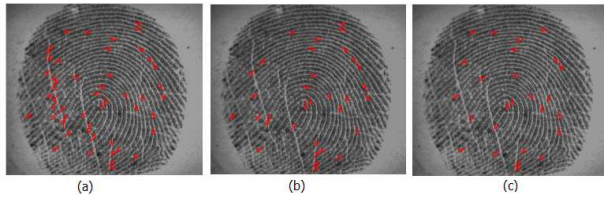


Figure 9: Results of minutiae filtering (a)No filtering (b)Wedge feature based filter (c)Gabor expansion based filter

References

- [1] author. paper about fingerprint feature extraction.
- [2] author. paper about quantifying image quality.
- [3] M. J. Bastiaans. *Gabors expansion of a signal into gaussian elementary signals*. Proceedings of the IEEE, 68:538–545, 1980.
- [4] A. M. Baze, G. T. B Verwaaijen, S. H. Garez, L. P. J. Veelunturf, and B. J. van der Zwaag. *A correlation-based fingerprint verification system*. In ProRISC2000 Workshops on Circuits, Systems and Signal Processing, Nov 2000.
- [5] Hung D. C. D. *Enhancement and feature purification of fingerprint images*. Pattern Recognition, 26(11):1661–1671, 1993.
- [6] Maio D. and Maltoni D. *Neural network based minutiae filtering in fingerprint images*. In 14th International Conference on Pattern Recognition, pages 1654–1658, 1998.
- [7] J. Daugman. *Complete discrete 2d gabor transform by neural networks for image analysis and compression*. Transactions on Acoustics, Speech and Signal Processing, 36:1169–1179, 1988.
- [8] O. R. Duda, P. E. Hart., and D. G. Stork. *Pattern Classification*. John Wiley and Sons, NY, 2001.
- [9] W. Freeman and E. Aldeman. *The design and use of steerable filters*. Transactions on PAMI, 13(9):891–906, 1991.
- [10] L. Hong, Y. Wang, and A. K. Jain. Transactions on PAMI, 21(4):777–789, August 1998.
- [11] Anil Jain, Salil Prabhakar, Lin Hong, and Sharath Pankanti. *Filterbank-based fingerprint matching*. In Transactions on Image Processing, volume 9, pages 846–859, May 2000.
- [12] Anil Jain, Arun Ross, and Salil Prabhakar. *Fingerprint matching using minutiae texture features*. In International Conference on Image Processing, pages 282–285, october 2001.
- [13] Tai Sing Lee. *Image representation using 2d gabor wavelets*. Transactions on PAMI, 18(10):959–971, 1996.
- [14] D. Maio and D. Maltoni. *Direct gray scale minutia detection in fingerprints*. Transactions on PAMI, 19(1), 1997.
- [15] Davide Maltoni. *Handbook of Fingerprint Recognition*. Springer Verlag, 2003.
- [16] Salil Prabhakar, Anil Jain, J. Wang, Sharath Pankanti, and Ruud Bolle. *Minutiae verification and classification for fingerprint matching*. In International Conference on Pattern Recognition, volume 1, pages 25–29, 2000.
- [17] Shie Qian and Dapang Chen. *Joint Time-Frequency Analysis, Methods and Applications*. Prentice Hall, 1996.
- [18] D. Maltoni R. Cappelli, D. Maio. *Synthetic fingerprint-image generation*. In International Conference on Pattern Recognition, 2000.
- [19] M. Riedmiller and H. Braun. *A direct adaptive method for faster backpropagation learning: The rprop algorithm*. In International Conference on Neural Networks, 1993.
- [20] Danny Rodberg, Colin Soutar, and B. V. K. Vijaya Kumar. *High-speed fingerprint verification using an optical correlator*. In Optical Pattern Recognition IX, volume 3386, pages 123–133, 1998.
- [21] E. P. Simoncelli and H. Farid. *Steerable wedge filters for local orientation analysis*. Transactions on Image Processing, 5(9), 1996.
- [22] Kritika Venkataramani and B. V. K. Vijaya Kumar. *Fingerprint verification using correlation filters*. Lecture Notes in Computer Science, 2668:886–894, August 2003.
- [23] Q. Xiao and H. Raafat. *Combining Statistical and Structural Information for Fingerprint Image Processing Classification and Identification*, pages 335–354. World Scientific, NJ, 1991.